Raman resonance tuning of quaterthiophene in filled carbon nanotubes at high pressures

R. S. Alencar[a,b,c,*], A. L. Aguiar[d], R. S. Ferreira[c], R. Chambard[e], B. Jousselme[f], J.-L. Bantignies[e], C. Weigel[e], S. Clément[e], R. Aznar[e], D. Machon[b,g], A. G. Souza Filho[c], A. San-Miguel[b,*], L. Alvarez[e,*]

[a] *Faculdade de Física, Universidade Federal do Pará, CEP 66075-110, Belém-PA, Brazil*
[b] *Univ Lyon, Université Claude Bernard Lyon 1, CNRS, Institut Lumière Matière, F-69622 LYON, France*
[c] *Departamento de Física, Centro de Ciências, Universidade Federal do Ceará, Fortaleza, Ceará, 60455-900 Brazil*
[d] *Departamento de Física, Universidade Federal do Piauí, 64049-550 Teresina, Piauí, Brazil*
[e] *Laboratoire Charles Coulomb UMR 5521, Université Montpellier 2, F-34095 Montpellier, France*
[f] *Université Paris-Saclay, CEA, CNRS, NIMBE, LICSEN, 91191, Gif-sur-Yvette, France.*
[g] *Laboratoire Nanotechnologies et Nanosystèmes (LN2), CNRS UMI-3463, Université de Sherbrooke, Institut Interdisciplinaire d'Innovation Technologique (3IT), Sherbrooke, Québec, Canada*

Abstract

Filling nanotubes with molecules is a route for the development of electronically modified one-dimensional hybrid structures for which the interplay between the electronic structure of molecules and nanotubes is a key factor. Tuning these energy levels with external parameters is an interesting strategy for the engineering of new devices and materials. Here we show that the hybrid system composed by quaterthiophene (4T) molecules confined

*corresponding author
Email addresses: rsalencar@ufpa.br (R. S. Alencar), alfonso.san-miguel-fuster@univ-lyon1.fr (A. San-Miguel), laurent.alvarez@umontpellier.fr (L. Alvarez)

in single-walled carbon nanotubes, presents a piezo-Raman-resonance of the molecule vibrational pattern. This behavior manifests as a rapid pressure induced enhancement of the 4T Raman mode intensities compared to the tubes G-band Raman modes. Density functional theory calculations allow to explain the spectral behaviour through the pressure-enhanced quaterthiophene resonance evolution. By increasing pressure, the tube cross-section deformation leads to a reduction of the intermolecular distance, to the splitting of the molecular levels and then to an increase of resonance opportunities. Calculations and experiments converge to the 4T piezo-resonance scenario associated with the pressure-induced nanotube radial collapse observed at about 0.8 GPa. Our findings offer possibilities for the development of pressure transducers based on molecule-filled carbon nanotubes.
Keywords: quaterthiophene, carbon nanotubes, resonance Raman spectroscopy, high pressure, straintronics.

2010 MSC: 00-01, 99-00

---

1. Introduction

A single-walled carbon nanotube (SWCNT) can be viewed as a rolled-up graphene nanoribbon constituting a hollow-core cylindrical shape of sp^2-hybridized carbon atoms, with electronic, optical and mechanical properties extremely dependent on diameter and the rolling angle or chirality [1, 2, 3, 4]. These unique physical properties have boosted carbon nanotubes (CNTs) to the scene of suitable materials for the nano-optoelectronic field [5, 6]. The functionalization of CNTs through the endohedral filling with molecules has been an efficient approach to develop new hybrid-one-dimensional (1D) structures. In such configuration, the host CNT prevents the guest molecules from mechanical and chemical degradation and contact with the enviroment, while

the guest molecules can modulate the energy band structure of CNTs and improve their emitting properties. In particular, the insertion of oligothiophene molecules into SWCNTs showed a photoluminescence (PL) emission in the visible spectral range with quantum yields up to 30% and a tunable electronic structure, which is dependent on the oligomer chain length [7, 8, 9]. On the other hand, the nanotube confinement is predicted to split the thiophene frontier orbitals due to the substantial molecular interchain interactions, which in turn modulate the electronic and absorption properties of the oligomers as well [10].

External parameters, as pressure, can be further used to tune the optical properties of nanomaterials [11, 12]. Specifically, in host-guest systems, high pressure is an effective manner to further modulate molecule-molecule and host-molecule interactions[13, 14], which offer opportunities for the fine-tuning of optoelectronic properties of quatertiophene (4T) filled SWCTNs (4T@SWCNTs) hybrid systems.

Resonance Raman spectroscopy (RRS) is an efficient tool for probing optical and electronic properties of carbon-based hybrid systems, since the Raman spectrum of carbon nanotubes is very sensitive to charge transfer (CT)[15, 16, 17, 18, 19], structural modification [20, 21, 22], defects [23, 24, 25] and doping [26, 27]. Actually, specifically for the 4T@SWCNT system, RRS has been used to show that the presence of the quaterthiophene induces a charge transfer between the guest 4T molecules and the host nanotubes. It was shown that CT scales with tube diameter and metallicity character [28, 29, 18, 19]. Furthermore, the supramolecular organization of the oligomer inside the CNT is deeply dependent on the CNT diameter and can favor the formation of strongly coupled J-aggregates (the molecules are stacked in pairs and aligned head-to-tail inside the nanotube) [30, 9].

In this work, we performed a combined high-pressure RRS experiments and DFT modelling on the hybrid 4T@SWCNTs system. Experiments were carried from ambient pressure conditions up to 10.7 GPa aiming to probe the interactions between tubes and oligomers. The rapid increase of the 4T Raman mode intensities relative to G-band allow to evidence a pressure-tuned thiophene resonance. Atomistic DFT calculations of the 1D-hybrid system under strain conditions shed light on the electronic structure evolution of both host and guest structures and support the interpretation of the experimental data.

2. Methodology

2.1. Samples and Experimental setup

A source of commercial electric arc SWCNTs (1.2 nm < diameter < 1.6 nm), called NT14 in the following, was used as the host material. Encapsulation of dimethyl-quaterthiophene ($C_{18}H_{14}S_4$) into carbon nanotubes was performed using a vapor reaction method previously described [19]. The hybrid material is named as 4T@NT14 in the following. The reference pristine nanotubes (NT14) have undergone the same thermal and cleaning treatments as the hybrid sample during the encapsulation process. Therefore, differences between the two samples can directly be attributed to the encapsulation of 4T molecules.

Raman experiments were carried out using a WITec system alpha300 equipped with laser excitation energies of 2.33 eV and 1.96 eV, for high-pressure measurements, and a Jobin Yvon T64000 spectrometer (in a triple mode), coupled to a charge-coupled detector, equipped with the 2.71, 2.54, 2.41, 2.33, 2.21 and 2.18 eV excitation energies, for ambient pressure experiments. The laser power was adjusted in order to improve the signal-to-noise ratio and to avoid heating effects on the samples. The laser beam was focused with a 50x (ambient pressure spectra) and a 20x (high-pressure spectra) objective lenses and the signal was dispersed by a grating of 1800 grooves/mm, resulting in a spectral resolution of $\sim \pm 1\ cm^{-1}$.

High pressures were achieved by using a National Bureau of Standards diamond-anvil cell type with a culet size of 700 μm. The 4T@NT14 and NT14 samples were loaded in a cylindrical pressure chamber, drilled in a pre-indented stainless steel gasket and placed between the two diamond anvils. NaCl powder was used as a pressure transmitting medium (PTM) in order to avoid any accidental filling of the tubes [4]. Pressure in the chamber was calibrated by the standard ruby luminescence R1 line method [31].

2.2. Theoretical methods

We used an LCAO-based DFT approach [32, 33] as implemented in the SIESTA code [34, 35] in order to calculate the electronic and structural properties of 4T@SWCNTs under uniaxial stress and probe in that way the effect of carbon nanotube deformation on the hybrid system properties. The Kohn-Sham orbitals were expanded in a double-ζ basis set composed of numerical pseudoatomic orbitals of finite range enhanced with polarization orbitals. Common atomic confinement determined by an energy shift

of 0.02 Ry was used to define the cutoff radius for the basis functions, while the fineness of the real space grid was determined by a mesh cutoff of 500 Ry [36]. For the exchange-correlation potential, we used the generalized gradient approximation (GGA) [37], and the pseudopotentials were modeled within the norm-conserving Troullier-Martins [38] scheme in the Kleinman-Bylander [39] factorized form. Brillouin-zone integrations were performed using a Monkhorst-Pack[40] grid of $1 \times 1 \times 10$ k-points for structural optimizations. For relative total energy, charge population analysis and projected density of states (PDOS) calculations, we used a grid of $1 \times 1 \times 40$ in order to obtain a good description of the energy levels and charge density. For each strained structural geometry relaxation, the SCF convergence thresholds for electronic total energy were set at 10^{-4} eV. Periodic boundary conditions were imposed in the a_z direction, while a set of perpendicular large enough (25 Å) off-plane lattice vectors, a_x and a_y, were set to prevent interactions between periodic images.

A semiconductor (17,0) SWCNT with a diameter of 1.33 nm was used to model the confinement of 4T molecules into CNTs. Such chirality was chosen to approach the mean diameter of the studied SWCNTs in our Raman spectroscopy experiments. Such specific chirality should not deeply influence our major findings since the critical pressure values for ovalization and collapse transformations of CNTs are not significantly dependent on the tube chirality but strongly dependent on its diameter [41].

We simulated five CNT unit cells (total length of 21.48Å) for this SWCNT in order to accommodate long 4T molecules (total length of 14.36Å) in the interior of tubes and avoid periodic image interaction. We should stress that the main effect of the encapsulating nanotube will be to promote a huge confinement for 4T molecules and subsequent radial compression of both 4T molecules in the interior of the tubes (as we will see later), emphasizing here that different chiralities and/or conducting properties will not deeply affect our results. For each deformation level, we fixed the atomic positions of a line of carbon atoms along the axial tube direction (the length of each CNT is kept constant because SWCNTs are more sensitive to radial than axial deformations), and the remaining atoms were fully relaxed for each strain level by using conjugated gradient techniques when the force was smaller than 0.05 eV/Å on each remained atoms. Such procedure can be justified due to the fact that CNTs have large Young's modulus values when compared with the critical pressures values for deforming their radial cross-section[42, 43, 44]. Therefore, we expect that radial deformation will be dominant even from

the first stages of pressure evolution. Besides that, the solid PTM used (NaCl power) is also expected to lose its hydrostaticity even for very low pressures[45], which certainly conduct to uniaxial stress on nanotube surface.

We define the uniaxial radial strain (ϵ_y) in the y-direction as (d_0-d)/d_0, where d_0 is the original diameter of the tube and d is the minimum wall-to-wall distance of the tube after applying the pressure-induced radial strain. We emphasize that since we are modeling uniaxial pressure by the constraint of a carbon atoms line, the pressure estimation will be still arbitrary and strong dependent of the atom's area (atom radius specifically) which was used. Even if we have information of the tube length and the residual force on each atom (for the constrained atoms), the exact area where this residual force is applied is not clear, and cannot be undoubtedly defined. Therefore, DFT estimations of pressure for isolated molecules and/or nanomaterials surface should be dealt with caution.

3. Results and discussion

Figure 1 (a) shows the measured Raman spectra of the NT14 (black lines) and 4T@NT14 (green lines) samples at some selected pressure values. These spectra are normalized by the G-band intensity. The complete pressure cycle is shown in Figure S1 (a) of Supplementary Information (SI). The spectra from 4T@NT14 sample present both 4T modes (1400-1530 cm^{-1}) [19, 18, 28] and the G-band of SWCNTs (1550-1600 cm^{-1}) while for NT14 sample, obviously, the spectra display only the G-band. In the 4T@NT14 system, the 4T mode intensities quickly increase for pressures above 0.4 GPa with respect to the G-band intensity. In contrast, in the empty SWCNTs sample, the G-band is well resolved up to 10.7 GPa, in spite of its broadening and intensity decrease as pressure increases.

In order to verify the role of the applied pressure on the resonance of the 4T@NT14 sample, we performed a Raman study of both hybrid and pristine samples as a function of the laser excitation energy. Figure 1 (b) shows that the intensity of quaterthiophene modes increases in comparison with G-band when the excitation energy is closer to the optical absorption of the oligomer (2.71 eV or 457.9 nm). A similar result has been observed by Alvarez et al. [19] and Almadori et al. [18], which attributed such behavior to two different origins: (i) 4T resonance effect, which increases the 4T Raman signal when approaching a resonance energy and (ii) a photoinduced charge transfer, that, in turn, changes the resonance conditions of the G-band, thus making its

intensity decrease. On the other hand, a recent study by Almadori et al. [28] have shown that such photoinduced charge transfer (an additional CT when 4T molecule is in resonance) only occurs in small diameter CNT (0.6 nm $<$ d $<$ 1 nm) while for large diameter CNT a permanent CT is observed. There is a striking similarity between the pressure response (Fig. 1 (a)) and the energy-excitation response (Fig. 1 (b)) on the 4T@NT14 spectra. This fact clearly points out that pressure application is tuning the resonance of photons used to excite the Raman spectra with electronic transitions of 4T molecules. Pressure then acts as a tuning parameter for molecular resonance in a similar way to laser energy tuning.

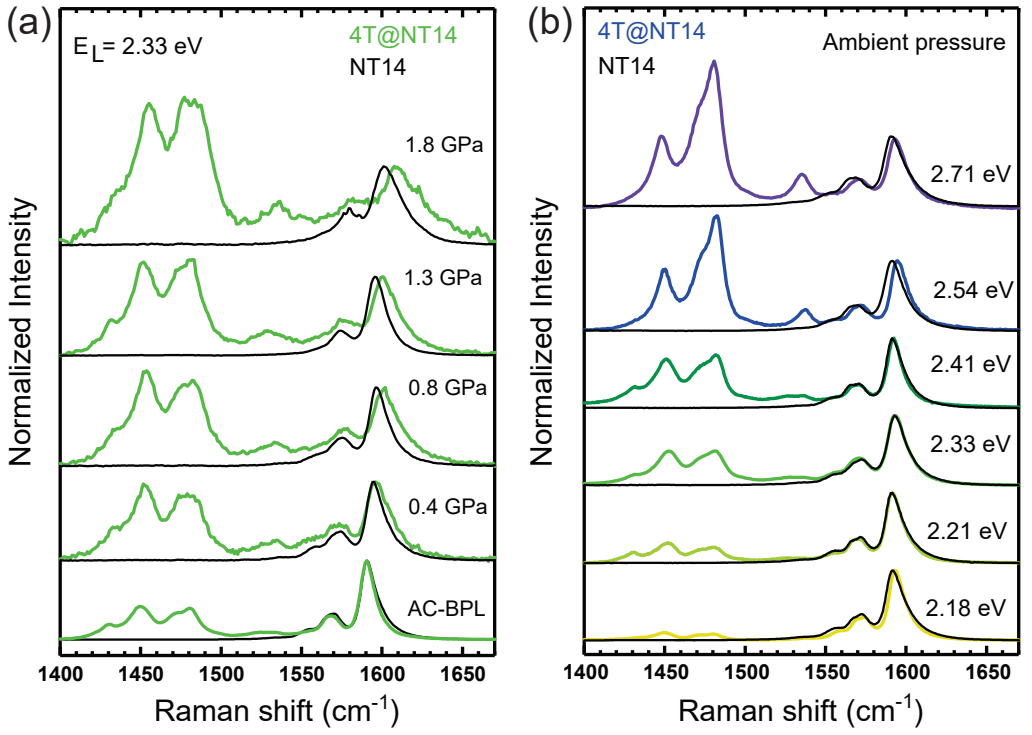

Figure 1: Pressure effect and excitation energy effect on the studied system. (a) Raman spectra collected at different pressures, excited with the energy of 2.33 eV both for empty SWCNTs (black lines) and 4T@SWCNTs hybrid system (green). AC-BPL correspond to ambient pressure conditions spectra before the pressure cycle. (b) Raman spectra of the same samples as in (a) at ambient pressure collected with different excitation energies with empty SWCNTs (black traces) and 4T@SWCNTs hybrid system (colorful lines). All data are normalized to the maximum of the G-band intensity.

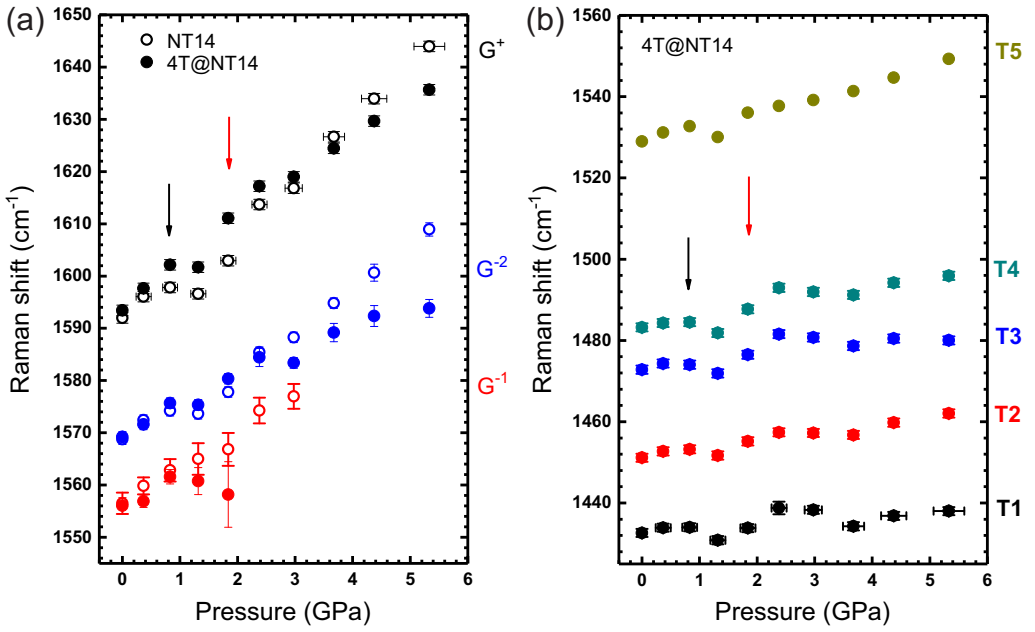

Figure 2: (a) G-band components for pristine SWCNTs (empty circles) and 4T@NT14 (filled circles) samples as a function of pressure. (b) 4T Raman frequencies for 4T@NT14 sample as a function of pressure. These data points were excited with the energy of 2.33 eV. The black and red arrows indicate the onset and the end of the pressure-induced collapse process.

To analyze the pressure-dependence of the 4T and SWCNTs signatures in 4T@NT14, we fitted the spectrum with eight Lorentzian components. The Raman peak positions at ambient pressure of these peaks are given in the Figure S3 (a) of SI. The higher energy 4T peaks are related to C=C stretching modes whereas the lower energy one is associated to C=C vibrations localized at the two outer quaterthiophene rings [19, 46, 47, 48, 49]. The G-band lineshape analysis was made by using three Lorentzian components (see Figure S3 (a) of SI for their ambient pressure Raman shift).

It has been shown that the G-band profile of carbon nanotubes is mainly characterized by two dominant peaks, named G^- and G^+, originated from the splitting of E_{2g} mode from graphite due to symmetry breaking, caused by nanotube curvature [50, 51, 52, 53, 54]. The higher-frequency band component (G^+) is known to be diameter independent, while the lower-frequency peak (G^-) decreases when decreasing the tube diameter [53, 54]. Therefore, we attributed the highest frequency component to the G^+ mode and the two lowest frequency peaks as being associated to G_1^- and G_2^- modes of different resonant set of tubes in the sample. These differences on the G^- frequencies come from the tube diameter dependence.

The G-band frequencies as a function of pressure for 4T@NT14 sample and empty NT14 system are shown in Figures 2 (a). We can see a similar trend for both systems. The G^+ and G^- components present a sudden downshift at ~ 0.8 GPa followed by a quasi-linear trend after 1.8 GPa. Similar behaviour is observed in the 4T modes, shown in Figure 2 (b). Therefore, there is no clear evidence of mechanical support provided by 4T molecules to increase the collapse pressure as it has been reported for SWCNT [4], DWCNT [55] and TWCNT bundles [20, 22] .

The observed downshift in the Raman signal at ~ 0.8 GPa is in very good agreement with the diameter dependent SWCNT collapse pressure given by the modified Lévy-Carrier scale law for SWCNT in Ref. [56]. It has been shown that variations of the tube cross-section can substantially modify the G-band spectra due to symmetry breaking and interatomic potential modifications [57]. A change on the sign of the pressure derivative ($\partial\omega/\partial P$) of the G-band has been attributed to the onset of nanotube radial collapse, while the end of the collapse process has been associated to a graphite-like evolution of G-band components [4, 21, 16, 22]. Accordingly, we associate the pressure values marked with black and red arrows in Fig. 2 as being the onset (~ 0.8 GPa) and the end (~ 1.8 GPa) of the radial collapse of the nanotube. In addition, the discontinuity of the 4T frequencies can be attributed to a

reorganization of the oligothiophene structure due to the tube cross-section ovalization during the collapse process. It is interesting to note that whereas small molecules as iodine, water or CO_2 can significantly alter the value of the SWCNT collapse pressure[14, 56, 58], we do not observe here an effect of 4T endohedral filling on the collapse pressure of the SWCNTs.

DFT calculations have been performed in order to understand how pressure application modifies the resonance of the 4T@SWCNT system. Firstly, the calculations were done for isolated 4T molecules aiming to study the interaction of two 4T molecules as a function of the intermolecular distance. Those calculations were conducted with 4T molecule atoms fixed in their isolated conformation. Band structure calculations based on density functional theory (DFT) with local (LDA) or gradient-corrected (GGA) exchange-correlation potentials are known to severely underestimate the band gap of semiconducting materials and also HOMO-LUMO gap of isolated systems [59]. Alternative approaches have been proposed to correct this issue such as DFT+U, Hybrid Functional and GW methods [60]. In our atomistic modelling, where 4T@SWCNTs systems are composed of hundred of atoms, such methods are computationally expensive. However, even if experimental values for HOMO-LUMO gap of quartertiophene molecules is estimated to be ~ 3.0 eV and the value obtained here with DFT framework is at around 1.9 eV (underestimation of 40%), we expected that qualitative tendencies of molecular levels as a function of compression rate of simulated nanotube are preserved [20].

In Figure 3 (a), we can see the two structural conformations of the 4T molecules wich were tested: *Config A* denotes the parallel approach of two 4T molecules but with lateral displacement. The *Config B* is used to describe the fully superposed parallel approaching of two 4T molecules. We note that at this stage we are not considering the effect of nanotube confinement.

Figure 3 (b) shows the evolution of the molecular gap (left axes) and binding energy (right axes) of 4T system as a function of intermolecular distance (d_{mol}) in the two considered configurations. As we can see, both configurations have minimum binding energy values when intermolecular distance is $d_{mol} = 4.32$ Å and they are both energetically stable (negative values) but *Config A* is clearly 0.1 eV more stable than *Config B* at this intermolecular distance. We can also see in Figure 3 (b) that the composed system has its molecular gap significantly decreases when the intermolecular distance is further reduced up to $d_{mol} = 3.00$ Å. Figure 3 (c) displays the molecular levels of the binary system and we can clearly see that the molecular gap is deeply reduced in *Config B*. For example, gap values changes from 1.82 eV (distant

molecules) to 1.45 eV (*Config A*) and to 0.42 eV (*Config B*) when intermolecular distance is $d_{mol} = 3.00$ Å. We can then conclude that the molecular gap can deeply change with the reduction of intermolecular distance which should take place under strong confinement or due to pressure effects. We note also that this gap reduction is driven by the splitting of molecular levels as the molecule-molecule interaction increases. This splitting takes place for both configuration but is more important in *Config B*.

Figure 4 (a) shows the results of an energy analysis for two 4T molecules now confined at the interior of an (17,0) nanotubes. We have seen that, outside the tube, *Config A* (4T molecules laterally shifted, see 3 (a)) is energetically more favorable than *Config B*. Inside a (17,0) tube the situation is different, as the 4T molecule and inner-wall van der Waals interaction becomes energetically dominant (see later). As a consequence, nanoconfinement constraints favor *Config B* which will majority exist in the interior of nanotubes with diameter of $\sim$ 1.32 nm (see S.I. Fig. S4). Therefore, we conducted calculations of two interacting 4T molecules in conformation *Config B* inside a (17,0) nanotube. The obtained results are compiled in Figure 4 (a). Even if it can be observed that there is a local minimum for two interacting 4T molecules in the center of the nanotube (intermolecular distance $d_{mol} = 3.50$ Å), we clearly observe that the best conformation for both 4T molecules is close to the tube inner surface (intermolecular distance $d_m = 6.50$ Å). It is important to note that such intermolecular distance of 6.50 Åis smaller than a twice of the molecule-to-molecule distance of 3.50 Åfor a second energetically stable conformation inside the 4T@(17,0) system. One can observe from the Fig. S4 (a) (where van der Waals radius is plotted along with the atomistic representations of the hybrid system) that a third molecule can not be easily accommodated between the two other 4T molecules, which necessarily will spent large energy cost followed by a strong nanotube cross-section deformation. Furthermore, from the experimental point of view, Almadori et al. [61] have shown for the 4T@NT14 sample that only two molecules can accommodate inner the NT14 nanotube. The obtained total energy difference of 4.2 eV between two minima values suggests that under no compression, 4T molecules will be adsorbed on the inner surface of nanotubes, similar to what has been observed in Ref. [29]. As discussed before, possible lateral displacements between two molecules (such as *Config A* and *Config B*) in the interior of nanotube will not be relevant when compared with the binding energy of one 4T molecule with inner nanotube surface, which is $\sim$ 4.0 eV higher. Therefore, we start our calculations under

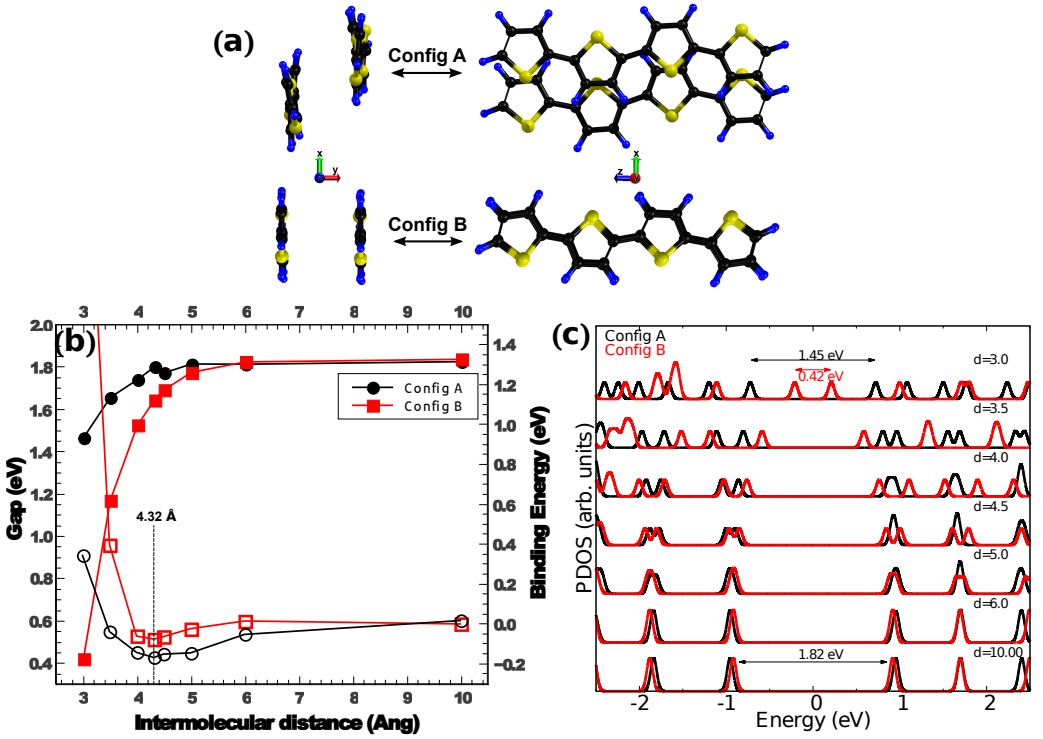

Figure 3: (a) Two isolated (non-encapsulated) 4T molecules in interaction as a function of intermolecular distance (measured along y-axis). In the first configuration, referred here as *Config A*, the 4T molecules are laterally displaced in the x-axis direction whereas in the second configuration, referred as *Config B*, the two 4T molecules overlap in this same directions. (b) Binding energy (open symbols, right axis) and molecular gap (filled symbols, left axis) as a function of the intermolecular distance. The vertical line denotes the energetically most stable distance for both isolated configurations (*Config A* and *Config B*). (c) Electronic levels of the composed 4T molecules as a function of intermolecular distance. The gap value changes as a function of intermolecular distance from 1.82 eV (d_{mol} =10.00 Å) to 1.45 eV (*Config A*) and to 0.42 eV (*Config B*) when intermolecular distance is fixed to d_{mol} =3.00 Å. See text for discussion. Energetic half distance between HOMO and LUMO levels for 4T molecules is set to zero.

compression, on this last conformation, where two 4T molecules are close to the inner tube surface.

In Figure 4 (b) we present the relaxed structures of hybrid 4T@(17,0) system for several strain rates. In this model, the 4T molecules are free to interact with the tube surface and with each other. We can clearly see in Figure 4 (b), that as the nanotube is compressed, that 4T molecules stabilize at distances from each other from $d_m = 6.56$ Å for $\epsilon_y = 0.00$ up to $d_m = 3.59$ Å for $\epsilon_y = 0.22$, which means that the nanotube induced compression pushes the two molecules to approach to each other. We expect then that under compression, the electronic structure of the hybrid 4T-nanotube system will deeply change and the results could be compared with the two molecules model (*Config B*) discussed above.

Figure 5 shows the projected density of states (PDOS) for the composed hybrid 2x4T@(17,0) system. Previous calculations on pristine (17,0) nanotubes (not shown here) have shown a band gap of 0.60 eV which is similar to that of Figure 5. PDOS on (17,0) nanotubes (black curves) obtained for $\epsilon_y = 0.04$ and PDOS on 4T molecules (red curves) are similar to energetic levels obtained for isolated systems (cf. Figure 3 (c)). However, after 4T molecule encapsulation, we can observe that 4T HOMO levels and top of the valence band of (17,0) nanotube are close to the Fermi level. PDOS also shows that the energetic difference between molecular levels for 4T molecules is 1.92 eV which is close to the molecular band gap for isolated 4T molecules in our DFT calculations. It is interesting to note that as the nanotube is compressed, energy levels split after $\epsilon_y = 0.16$ (d_{mol}= 4.55 Å). Such electronic energy splitting is also observed for isolated molecules in *Config B* of Figure 3 (c) at the same d_{mol} value. We may note that the splitting of HOMO and LUMO levels develops with pressure application, but with an amplitude which is smaller in the encapsulated configuration, where contrarily to this case, the structure was not allowed to relax. In any case, the compression of (17,0) nanotube reduces the 4T molecular gap (develops an energy level splitting) due to the interaction between the 4T molecules. The splitting of the molecular levels offers new opportunities for spectroscopic resonance as it is observed in our experiments. At the maximum of the applied strain (ϵ_y =0.22, $d_{mol} = 3.59$ Å) the molecular gap reduces to 1.35 eV, i.e., a contraction of ~ 30 %.

Our calculations allow to propose a scenario to explain the fast pressure induced 4T/NT14 Raman intensity ratio evolution. With increasing pressure, the tube cross-section deforms and the intermolecular distance d_m

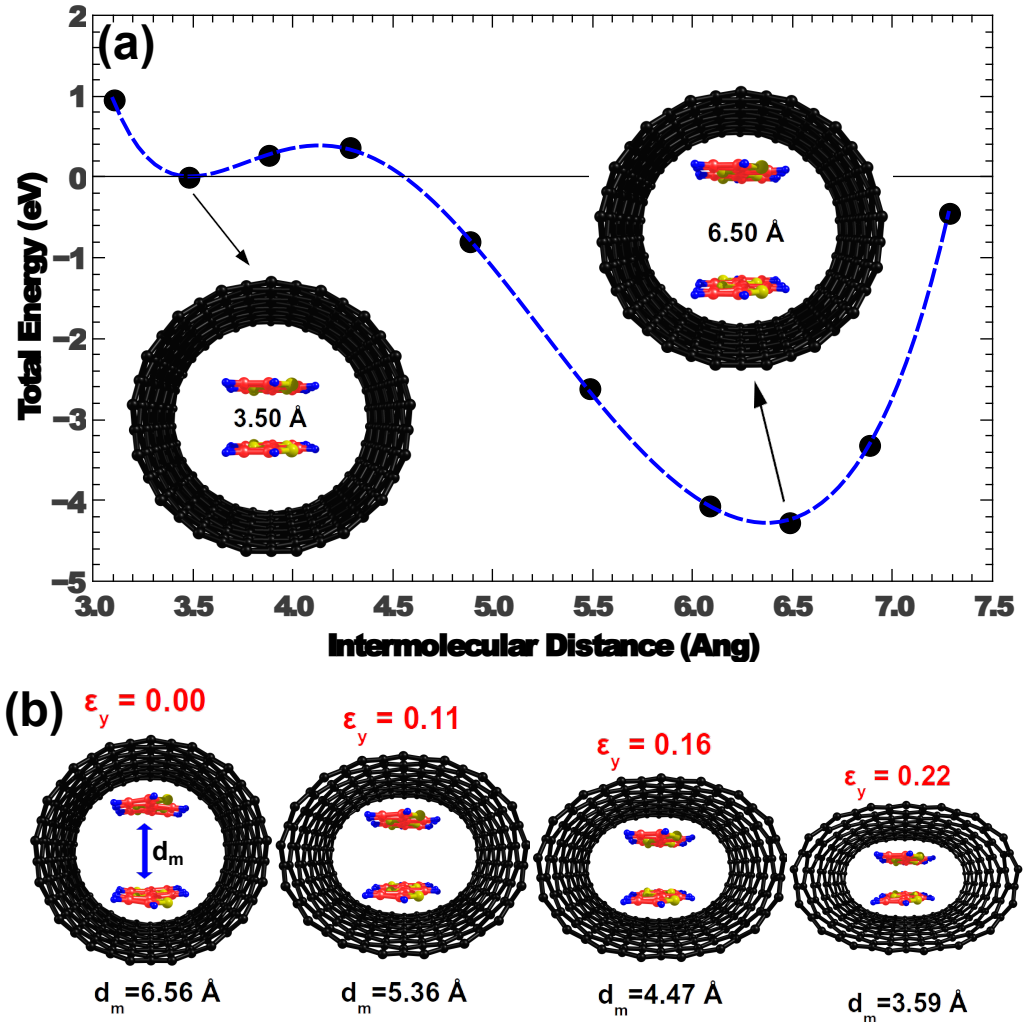

Figure 4: (a) Total energy of two 4T molecules confined in (17,0) SWCNT nanotube (4T@(17,0)) in the absence of strain. Calculations of relative energy were conducted with the intermolecular distance fixed ranging from $d_{mol} = 3.0$ Å up to $d_{mol} = 7.3$ Å. A local minimum was obtained at $d_{mol} = 3.5$ Å and the global minimum at $d_{mol} = 6.5$ which correspond to two 4T molecules close to inner surface of nanotubes. The dashed blue line is a 6^{th} order polynomial fit just to guide the eyes. (b) Snapshots of cross-section view of two 4T encapsulated at (17,0) SWCNT under uniaxial deformation from $\epsilon_y = 0.00$ (intermolecular distance $d_{mol} = 6.56$ Å) up to $\epsilon_y = 0.22$ (intermolecular distance $d_{mol} = 3.59$ Å).

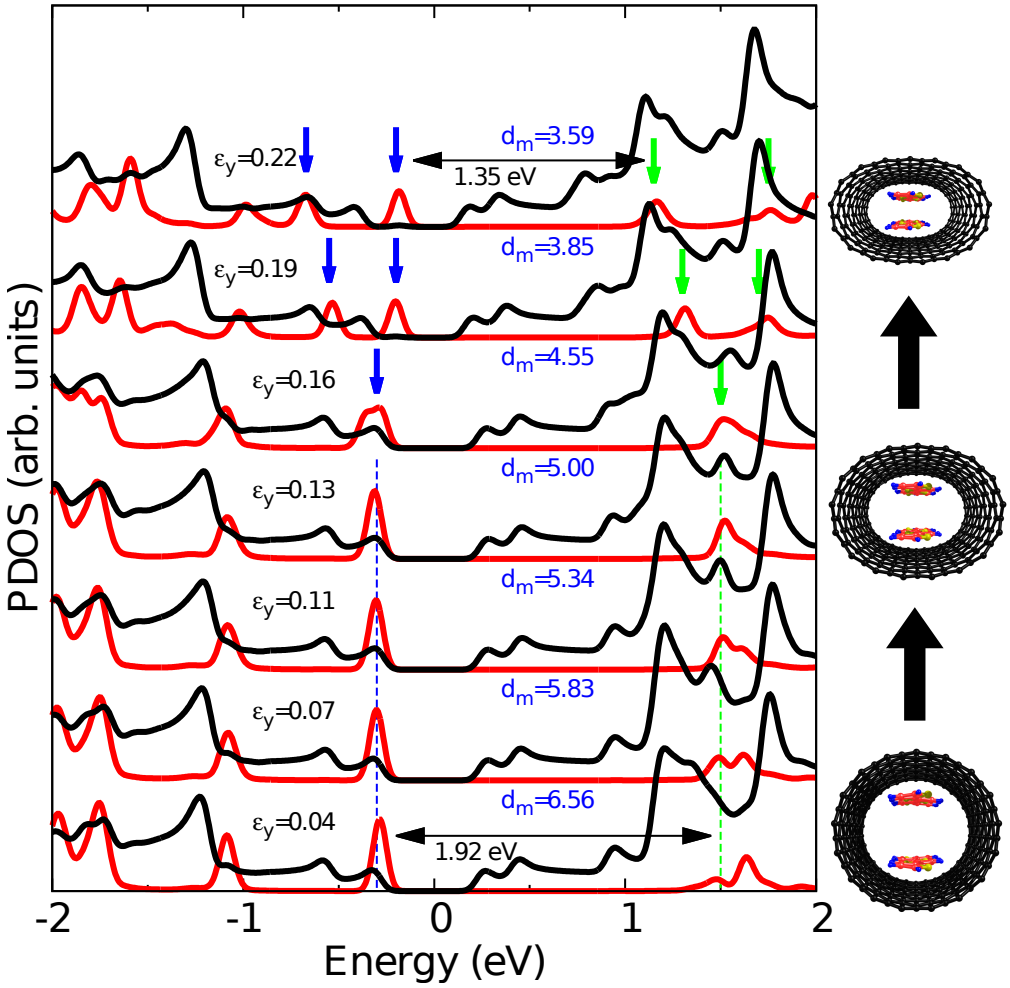

Figure 5: Projected Density of States (PDOS) on nanotube (17,0) SWCNT (black curves) and on 4T molecules (red curves) for the composed 4T@(17,0) system as a function of strain compression (ε_y). Blue and green arrows denote the splitting of HOMO and LUMO levels respectively of 4T molecules. The 4T molecular gap can be seen changing from 1.92 eV up to 1.35 eV as the hybrid 4T@(17,0) is compressed. Relaxed 4T intermolecular distance d_m (in Å) for each level of nanotube compression is also shown (blue values). Fermi level is set to zero.

decreases, which in turn decreases the quaterthiophene electronic gap. As a consequence, the molecule enters in resonance with lower laser excitation energies in comparison to ambient pressure conditions. This may lead in principle to charge transfer processes associated with the 4T resonant absorption process coupled with the tube-4T proximity.

In order to verify if an additional charge is transferred to nanotubes when the 4T molecule resonance is tuned by pressure, we performed a high-pressure Raman experiment on 4T@NT14 sample, but using an excitation energy of 1.96 eV far from 4T resonance. There is no significant difference with respect to our observations with the 2.33 eV excitation. We conclude that the G-band does not allow to detect CT associated to 4T filling, in complete agreement to the report by Almadori et al. [28] (See Fig. S1 (b) to (c) of SI for details). We have analyzed the pressure evolution of the G-band's area for the two excitation energies (1.96 and 2.33 eV) in the 4T@NT14 and compared it to the pristine NT14 sample. For this purpose all spectra were normalized by the integration time (see Fig S1(a)) and we set all ambient conditions spectra to the same unity area of the G-band. Figure 6 shows the obtained results. We observe that in the empty tube, the G-band area rapidly decreases from the first compression stages, reaching then a very low intensity. In the case of 4T filling we observe that the G-band area increases at first stages of compression before following a similar trend than the empty nanotubes, but with a higher intensity in the region between 1 and 3 GPa. This is even more evident for the 1.96 eV excitation where a higher intensity is observed until 7 GPa. All these observations can be explained through a resonance enhancement associated to the 4T molecules encapsulation. We will see in the following that the RBM, which has more constrained resonant conditions, does not either allow the unambiguous detection of a charge transfer effect or intensity bursts.

Figure 7 (a) shows the RBM part of the spectra for the NT14 (black lines) and the 4T@NT14 (light green lines) samples for pressure ranging from ambient to 10.7 GPa. Two RBM peaks (related to different tube diameters) can be observed for each one of the samples (see ambient pressure values in Figure S3 (b) of SI). These two RBM modes disappear above $\sim$ 3.0 GPa (R1) and $\sim$ 9.9 GPa (R2) for the pristine sample, whereas for 4T@NT14 system the corresponding pressure are much lower: $\sim$ 0.8 GPa (R1') and $\sim$ 1.3 GPa (R2').

The RBM peaks lineshape analysis was performed by using one Lorentzian component for each RBM mode, similar to previous works in SWCNTs

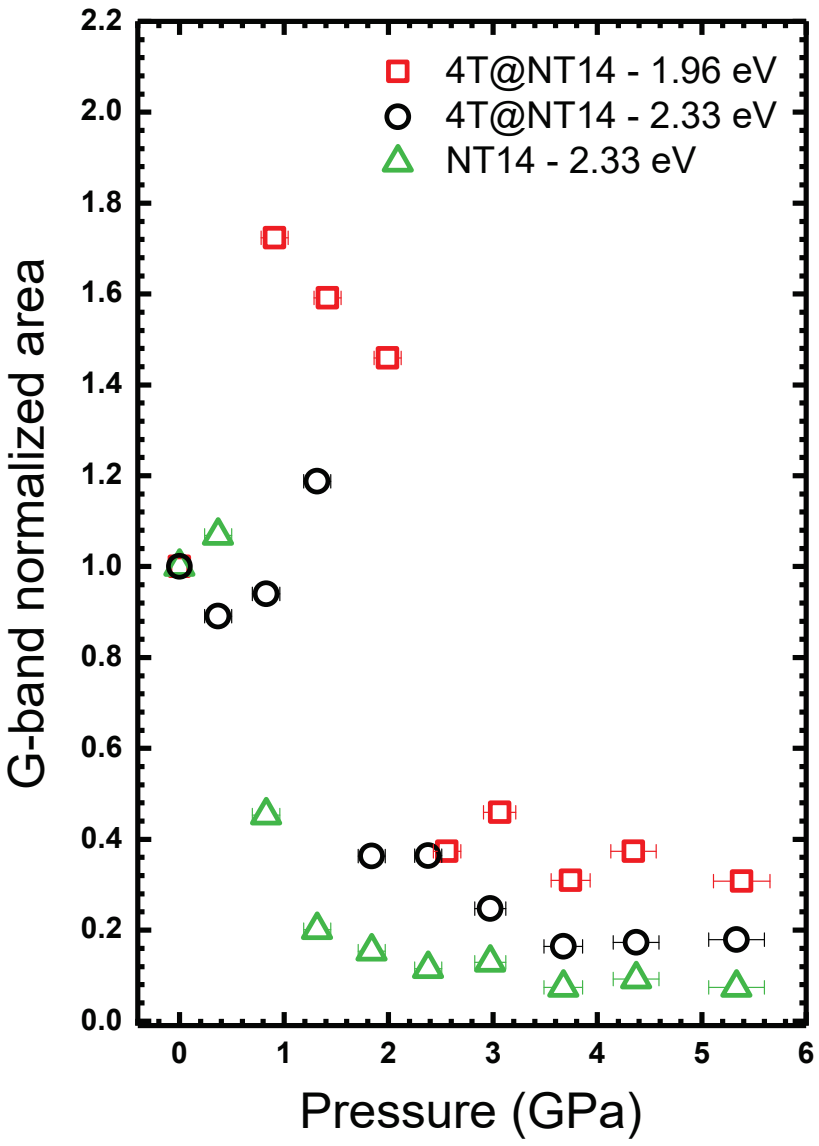

Figure 6: Integration time normalized G-band area relative to the G-band area at ambient pressure as a function of pressure for NT14 (light green triangles) and 4T@NT14 systems (black circles) excited with 2.33 eV. The red squares represent the normalized G-band area of 4T@NT14 system excited with 1.96 eV.

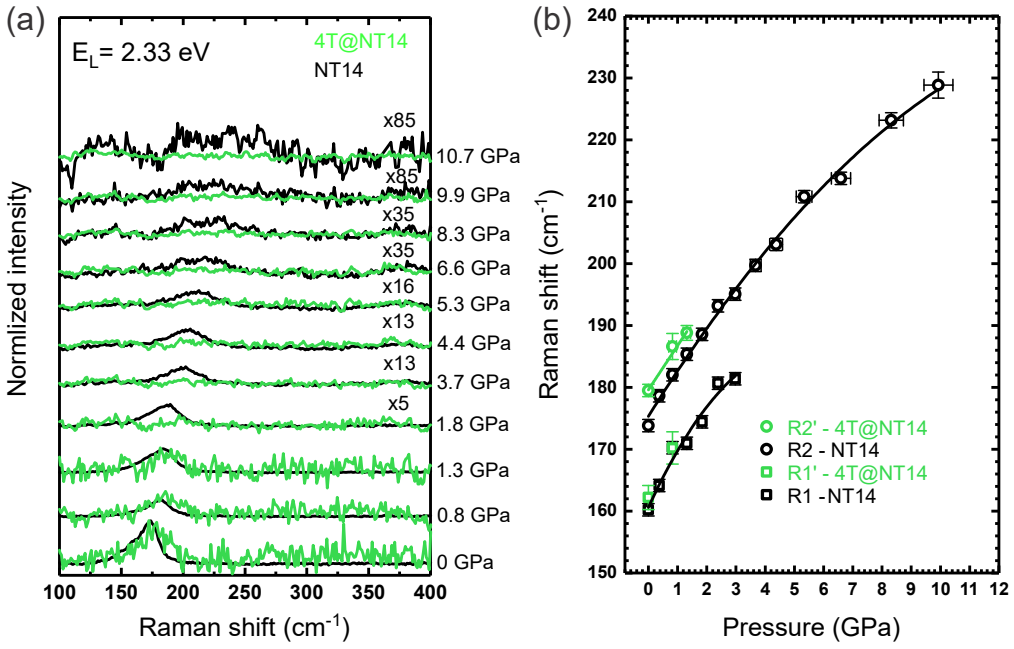

Figure 7: (a) RBM Raman spectra collected at different pressures with excitation energy of 2.33 eV for empty NT14 (black lines) and 4T@NT14 (light green lines) systems. All spectra were normalized by the integration time, and after that for comparison, the 4T@NT14 (NT14) spectra were normalized by the R2'(R2) intensity at ambient condition 0.15 (2.36). (b) RBM Raman frequencies of the two peaks in empty NT14 (R1 and R2) and 4T@NT14 composite (R1' and R2') as a function of pressure.

[4, 62, 63]. RBM Raman frequencies vs. pressure plot is shown in Figure 7 (b). The R1 and R2 peak frequencies are well fitted by second-degree polynomials [56]. Despite the fast dropping on the intensities of R1' and R2' modes, the pressure evolution of their positions is similar to that of R1 and R2 modes.

Resonance Raman spectra of CNTs are strongly affected by pressure. In particular, attenuation of the RBM signal has been attributed either to loss of tube resonance, that is caused by changes in the electronic transition energies due to pressure-induced structural modifications [64], or to radial tube collapse [20, 64, 65, 66, 4, 56]. Aguiar et al. [67] have observed that after the tube collapse process, the RBM frequencies of SWCNTs spread over a large frequency range but can still be observed well above the collapse pressure. Although the RBM signature is visible up to 10 GPa for NT14 sample, the full width at half maximum (FWHM) (Figure S2 (a) of SI) increases rapidly for pressure values beyond 1.8 GPa, i.e, the collapse pressure, in complete agreement with G-band behaviour.

It has been observed that the presence of molecules inside SWCNTs does not modify strongly the maximum pressure up to which the RBM signal can be measured. This has been shown for instance in water filling[4] or fullerene C_{70} filling[68]. In the case of 4T filling, we observe a strong attenuation of the RBM at much lower pressures than for the pristine sample. A similar result is observed for the 4T@NT14 sample excited with 1.96 eV (see Figures S3 (b)-(c)), where the RBM peaks disappear after pressure where the collapse occurs. This observation is then clearly in line with a pressure-induced resonance evolution due to the 4T filling.

Even at ambient pressure, the presence of 4T molecules into SWCNTs has been shown to drastically change the tube RBM signature. Depending on the molecular organization of 4T confined into SWCNT and the laser excitation energy, the RBM peaks can undergo an up-shift or even a significant loss of their intensity [69, 19, 18]. The magnitude of the RBM up-shift increases when the number of oligomer increases in a section of the tube and the closeness between SWCNT and 4T decreases. On the other hand, as the laser excitation energy is closer to the optical absorption of quaterthiophene, the loss of RBM intensity is more pronounced due to the photoinduced charge transfer from 4T to SWCNT [18, 28, 19]. We can then attribute the fast attenuation of the RBM vibrational modes in the 4T@NT14 system, with respect to the pristine one, either to radial tube collapse or to a charge transfer from 4T to SWCNT during the collapse process. Both processes

could also contribute to the observed phenomenon. The narrower resonance conditions needed for RBM resonance may explain a higher sensitivity to charge transfer which was not detected from G-band. We can not exclude that the RBM signal of the post-collapsed 4T@NT14 systems may be silenced due to the enhanced 4T-SWCNT interaction at collapse without participation of CT processes.

4. Conclusions

We have shown that high pressure allows to tune the interaction of quaterthiophene endohedral molecules in SWCNTs. Such interactions, between the molecules themselves and with the nanotube-walls lead to strong changes in the molecule electronic structure. As a consequence, the molecule photon absorption resonance conditions can be strongly modified through the carbon nanotube pressure-induced radial deformation. A strong enhancement of the molecule Raman resonance is then obtained at high pressures. We have shown that such enhancement presents strong similarities to laser energy Raman resonance tuning thus offering novel opportunities for the development of pressure transducers based on molecule-filled carbon nanotubes.

Acknowledgments

The authors acknowledge Central Analítica-UFC/CT-INFRA-FINEP/Pro-Equipamentos-CAPES/CNPq-SisNano-MCTI 2019 (Grant 442577/2019-2) for Raman measurements. The authors acknowledge the support from CAPES-COFECUB project Ph938/19 and 88881.192341/2018-01.

References

[1] R. Saito, G. Dresselhaus, M. S. Dresselhaus, Physical Properties of Carbon Nanotubes, Published by imperial college press and distributed by world scientific publishing co., 1998. arXiv:https://www.worldscientific.com/doi/pdf/10.1142/p080, doi:10.1142/p080. URL https://www.worldscientific.com/doi/abs/10.1142/p080

[2] A. Jorio, M. S. Dresselhaus, G. Dresselhaus, Carbon nanotubes: advanced topics in the synthesis, structure, properties and applications, Springer, 2008.

[3] M. Dresselhaus, G. Dresselhaus, A. Jorio, Unusual properties and structure of carbon nanotubes, Annu. Rev. Mater. Res. 34 (1) (2004) 247–278. arXiv:http://dx.doi.org/10.1146/annurev.matsci.34.040203.114607, doi:10.1146/annurev.matsci.34.040203.114607.
URL http://dx.doi.org/10.1146/annurev.matsci.34.040203.114607

[4] A. C. Torres-Dias, S. Cambré, W. Wenseleers, D. Machon, A. San-Miguel, Chirality-dependent mechanical response of empty and water-filled single-wall carbon nanotubes at high pressure, Carbon (2015) 442–541doi:10.1016/j.carbon.2015.08.032.
URL http://www.sciencedirect.com/science/article/pii/S0008622315301512

[5] P. Avouris, M. Freitag, V. Perebeinos, Carbon-nanotube photonics and optoelectronics, Nature Photonics 2 (2008) 341 EP –, review Article.
URL https://doi.org/10.1038/nphoton.2008.94

[6] J. A. Misewich, R. Martel, P. Avouris, J. C. Tsang, S. Heinze, J. Tersoff, Electrically induced optical emission from a carbon nanotube fet, Science 300 (5620) (2003) 783–786. arXiv:https://science.sciencemag.org/content/300/5620/783.full.pdf, doi:10.1126/science.1081294.
URL https://science.sciencemag.org/content/300/5620/783

[7] J. Gao, P. Blondeau, P. Salice, E. Menna, B. Bártová, C. Hébert, J. Leschner, U. Kaiser, M. Milko, C. Ambrosch-Draxl, M. A. Loi, Electronic interactions between pea and pod : The case of oligothiophenes encapsulated in carbon nanotubes, Small 7 (13) (2011) 1807–1815. arXiv:https://onlinelibrary.wiley.com/doi/pdf/10.1002/smll.201100319, doi:10.1002/smll.201100319.
URL https://onlinelibrary.wiley.com/doi/abs/10.1002/smll.201100319

[8] M. A. Loi, J. Gao, F. Cordella, P. Blondeau, E. Menna, B. Bártová, C. Hébert, S. Lazar, G. A. Botton, M. Milko, C. Ambrosch-Draxl, Encapsulation of conjugated oligomers in single-walled carbon nanotubes: Towards nanohybrids for photonic devices, Advanced Materials 22 (14) (2010) 1635–1639. arXiv:https:

//onlinelibrary.wiley.com/doi/pdf/10.1002/adma.200903527, doi:10.1002/adma.200903527.
URL https://onlinelibrary.wiley.com/doi/abs/10.1002/adma.200903527

[9] E. Gaufrès, N. Y. W. Tang, A. Favron, C. Allard, F. Lapointe, V. Jourdain, S. Tahir, C.-N. Brosseau, R. Leonelli, R. Martel, Aggregation control of a-sexithiophene via isothermal encapsulation inside single-walled carbon nanotubes, ACS Nano 10 (11) (2016) 10220–10226. doi:10.1021/acsnano.6b05660.
URL https://doi.org/10.1021/acsnano.6b05660

[10] T. Yumura, H. Yamashita, Modulating the electronic properties of multimeric thiophene oligomers by utilizing carbon nanotube confinement, The Journal of Physical Chemistry C 118 (10) (2014) 5510–5522. arXiv:https://doi.org/10.1021/jp5006555, doi:10.1021/jp5006555.
URL https://doi.org/10.1021/jp5006555

[11] F. Medeghini, M. Hettich, R. Rouxel, S. D. Silva Santos, S. Hermelin, E. Pertreux, A. Torres Dias, F. Legrand, P. Maioli, A. Crut, F. Vallée, A. San Miguel, N. Del Fatti, High-pressure effect on the optical extinction of a single gold nanoparticle, ACS Nano 12 (10) (2018) 10310–10316. arXiv:https://doi.org/10.1021/acsnano.8b05539, doi:10.1021/acsnano.8b05539.
URL https://doi.org/10.1021/acsnano.8b05539

[12] D. Machon, V. Pischedda, S. Le Floch, A. San-Miguel, Perspective: High pressure transformations in nanomaterials and opportunities in material design, Journal of Applied Physics 124 (16) (2018) 160902. arXiv:https://doi.org/10.1063/1.5045563, doi:10.1063/1.5045563.
URL https://doi.org/10.1063/1.5045563

[13] A. L. Aguiar, E. B. Barros, V. P. Sousa Filho, H. Terrones, V. Meunier, D. Machon, Y. A. Kim, H. Muramatsu, M. Endo, F. Baudelet, A. San-Miguel, A. G. Souza Filho, Pressure tuning of bromine ionic states in double-walled carbon nanotubes, The Journal of Physical Chemistry C 121 (19) (2017) 10609–10619. arXiv:https://doi.org/10.1021/acs.jpcc.7b03187, doi:10.1021/acs.jpcc.7b03187.
URL https://doi.org/10.1021/acs.jpcc.7b03187

[14] L. Alvarez, J.-L. Bantignies, R. Le Parc, R. Aznar, J.-L. Sauvajol, A. Merlen, D. Machon, A. San Miguel, High-pressure behavior of polyiodides confined into single-walled carbon nanotubes: A raman study, Phys. Rev. B 82 (2010) 205403. doi:10.1103/PhysRevB.82.205403.

[15] A. Forestier, F. Balima, C. Bousige, G. d. S. Pinheiro, R. Fulcrand, M. Kalbáč, D. Machon, A. San-Miguel, Strain and piezo-doping mismatch between graphene layers, The Journal of Physical Chemistry C 124 (20) (2020) 11193–11199. arXiv:https://doi.org/10.1021/acs.jpcc.0c01898, doi:10.1021/acs.jpcc.0c01898.
URL https://doi.org/10.1021/acs.jpcc.0c01898

[16] W. Neves, R. Alencar, R. Ferreira, A. Torres-Dias, N. Andrade, A. San-Miguel, Y. Kim, M. Endo, D. Kim, H. Muramatsu, A. Aguiar, A. S. Filho, Effects of pressure on the structural and electronic properties of linear carbon chains encapsulated in double wall carbon nanotubes, Carbon 133 (2018) 446 – 456. doi:https://doi.org/10.1016/j.carbon.2018.01.084.
URL http://www.sciencedirect.com/science/article/pii/S0008622318300939

[17] L. G. Moura, L. M. Malard, M. A. Carneiro, P. Venezuela, R. B. Capaz, D. Nishide, Y. Achiba, H. Shinohara, M. A. Pimenta, Charge transfer and screening effects in polyynes encapsulated inside single-wall carbon nanotubes, Phys. Rev. B 80 (2009) 161401. doi:10.1103/PhysRevB.80.161401.
URL https://link.aps.org/doi/10.1103/PhysRevB.80.161401

[18] Y. Almadori, L. Alvarez, R. Arenal, R. Babaa, T. Michel, R. Le Parc, J.-L. Bantignies, B. Jouselme, S. Palacin, P. Hermet, J.-L. Sauvajol, Charge transfer in conjugated oligomers encapsulated into carbon nanotubes, physica status solidi (b) 248 (11) (2011) 2560–2563. doi:10.1002/pssb.201100094.
URL http://dx.doi.org/10.1002/pssb.201100094

[19] L. Alvarez, Y. Almadori, R. Arenal, R. Babaa, T. Michel, R. Le Parc, J.-L. Bantignies, B. Jousselme, S. Palacin, P. Hermet, J.-L. Sauvajol, Charge transfer evidence between carbon nanotubes and encapsulated conjugated oligomers, The Journal of Physical Chemistry C 115 (24)

(2011) 11898–11905. arXiv:http://dx.doi.org/10.1021/jp1121678, doi:10.1021/jp1121678.
URL http://dx.doi.org/10.1021/jp1121678

[20] R. S. Alencar, A. L. Aguiar, A. R. Paschoal, P. T. C. Freire, Y. A. Kim, H. Muramatsu, M. Endo, H. Terrones, M. Terrones, A. San-Miguel, M. S. Dresselhaus, A. G. Souza Filho, Pressure-Induced Selectivity for Probing Inner Tubes in Double- and Triple-Walled Carbon Nanotubes: A Resonance Raman Study, J. Phys. Chem. C 118 (15) (2014) 8153–8158. doi:{10.1021/jp4126045}.

[21] R. Alencar, W. Cui, A. Torres-Dias, T. F. Cerqueira, S. Botti, M. A. Marques, O. Ferreira, C. Laurent, A. Weibel, D. Machon, D. Dunstan, A. S. Filho, A. San-Miguel, Pressure-induced radial collapse in few-wall carbon nanotubes: A combined theoretical and experimental study, Carbon 125 (2017) 429 – 436. doi:https://doi.org/10.1016/j.carbon.2017.09.044.
URL http://www.sciencedirect.com/science/article/pii/S0008622317309193

[22] S. Silva-Santos, R. Alencar, A. Aguiar, Y. Kim, H. Muramatsu, M. Endo, N. Blanchard, A. San-Miguel, A. Souza Filho, From high pressure radial collapse to graphene ribbon formation in triple-wall carbon nanotubes, Carbon 141 (2019) 568–579. doi:10.1016/j.carbon.2018.09.076.
URL https://www.scopus.com/inward/record.uri?eid=2-s2.0-85054721781&doi=10.1016%2fj.carbon.2018.09.076&partnerID=40&md5=ff6ec8c9f31880af81e1cbb133ae0f83

[23] M. S. Dresselhaus, A. Jorio, A. G. Souza Filho, R. Saito, Defect characterization in graphene and carbon nanotubes using raman spectroscopy, Philosophical Transactions of the Royal Society A: Mathematical, Physical and Engineering Sciences 368 (1932) (2010) 5355–5377. arXiv:https://royalsocietypublishing.org/doi/pdf/10.1098/rsta.2010.0213, doi:10.1098/rsta.2010.0213.
URL https://royalsocietypublishing.org/doi/abs/10.1098/rsta.2010.0213

[24] F. Côa, M. Strauss, Z. Clemente, L. L. R. Neto, J. R. Lopes, R. S. Alencar, A. G. S. Filho, O. L. Alves, V. L. S. Castro, E. Bar-

bieri, D. S. T. Martinez, Coating carbon nanotubes with humic acid using an eco-friendly mechanochemical method: Application for cu(ii) ions removal from water and aquatic ecotoxicity, Science of The Total Environment 607-608 (2017) 1479 – 1486. doi:https://doi.org/10.1016/j.scitotenv.2017.07.045.
URL http://www.sciencedirect.com/science/article/pii/S0048969717317485

[25] Y. Miyata, K. Mizuno, H. Kataura, Purity and defect characterization of single-wall carbon nanotubes using raman spectroscopy, Journal of Nanomaterials 2011 (2011) 7.
URL 10.1155/2011/786763

[26] M. Kalbac, H. Farhat, L. Kavan, J. Kong, M. S. Dresselhaus, Competition between the spring force constant and the phonon energy renormalization in electrochemically doped semiconducting single-walled carbon nanotubes, Nano Letters 8 (10) (2008) 3532–3537. arXiv:https://doi.org/10.1021/nl801637h, doi:10.1021/nl801637h.
URL https://doi.org/10.1021/nl801637h

[27] J. C. Tsang, M. Freitag, V. Perebeinos, J. Liu, P. Avouris, Doping and phonon renormalization in carbon nanotubes, Nature Nanotechnology 2 (11) (2007) 725–730. doi:10.1038/nnano.2007.321.
URL https://doi.org/10.1038/nnano.2007.321

[28] Y. Almadori, G. Delport, R. Chambard, L. Orcin-Chaix, A. Selvati, N. Izard, A. Belhboub, R. Aznar, B. Jousselme, S. Campidelli, P. Hermet, R. L. Parc, T. Saito, Y. Sato, K. Suenaga, P. Puech, J. Lauret, G. Cassabois, J.-L. Bantignies, L. Alvarez, Fermi level shift in carbon nanotubes by dye confinement, Carbon 149 (2019) 772 – 780. doi:https://doi.org/10.1016/j.carbon.2019.04.041.
URL http://www.sciencedirect.com/science/article/pii/S0008622319303756

[29] A. Belhboub, P. Hermet, L. Alvarez, R. Le Parc, S. Rols, A. C. Lopes Selvati, B. Jousselme, Y. Sato, K. Suenaga, A. Rahmani, J.-L. Bantignies, Enhancing the infrared response of carbon nanotubes from oligoquaterthiophene interactions, The Journal of Physical Chemistry C 120 (50) (2016) 28802–28807. arXiv:https://doi.org/10.1021/acs.

jpcc.6b09329, doi:10.1021/acs.jpcc.6b09329.
URL https://doi.org/10.1021/acs.jpcc.6b09329

[30] E. Gaufrès, N. Y. W. Tang, F. Lapointe, J. Cabana, M.-A. Nadon, N. Cottenye, F. Raymond, T. Szkopek, R. Martel, Giant raman scattering from j-aggregated dyes inside carbon nanotubes for multispectral imaging, Nature Photonics 8 (2013) 72 EP –.
URL https://doi.org/10.1038/nphoton.2013.309

[31] H. Mao, J. Xu, P. Bell, Calibration of the ruby pressure gauge to 800-kbar under quasi-hydrostatic conditions, J. Geophys. Res. 91 (B5) (1986) 4673–4676. doi:10.1029/JB091iB05p04673.

[32] P. Hohenberg, W. Kohn, Inhomogeneous electron gas, Phys. Rev. 136 (1964) B864–B871. doi:10.1103/PhysRev.136.B864.
URL http://link.aps.org/doi/10.1103/PhysRev.136.B864

[33] W. Kohn, L. J. Sham, Self-consistent equations including exchange and correlation effects, Phys. Rev. 140 (1965) A1133–A1138. doi:10.1103/PhysRev.140.A1133.
URL http://link.aps.org/doi/10.1103/PhysRev.140.A1133

[34] P. Ordejón, E. Artacho, J. M. Soler, Self-consistent order-n density-functional calculations for very large systems, Phys. Rev. B 53 (1996) 10441.

[35] D. Sánchez-Portal, E. Artacho, J. M. Soler, Density-functional method for very large systems with LCAO basis sets, Int. J. Quantum Chem. 65 (1997) 453.

[36] E. Anglada, J. M. Soler, J. Junquera, E. Artacho, Systematic generation of finite-range atomic basis sets for linear-scaling calculations, Phys. Rev. B 66 (2002) 205101. doi:10.1103/PhysRevB.66.205101.
URL http://link.aps.org/doi/10.1103/PhysRevB.66.205101

[37] J. P. Perdew, K. Burke, M. Ernzerhof, Generalized gradient approximation made simple, Phys. Rev. Lett. 77 (1996) 3865–3868. doi:10.1103/PhysRevLett.77.3865.
URL https://link.aps.org/doi/10.1103/PhysRevLett.77.3865

[38] N. Troullier, J. L. Martins, Efficient pseudopotentials for plane-wave calculations, Phys. Rev. B 43 (1991) 1993.

[39] L. Kleinman, D. M. Bylander, Efficacious form for model pseudopotentials, Phys. Rev. Lett. 48 (1982) 1425–1428. doi:10.1103/PhysRevLett.48.1425.
URL https://link.aps.org/doi/10.1103/PhysRevLett.48.1425

[40] H. J. Monkhorst, J. D. Pack, Special points for brillouin-zone integrations, Phys. Rev. B 13 (1976) 5188–5192. doi:10.1103/PhysRevB.13.5188.
URL https://link.aps.org/doi/10.1103/PhysRevB.13.5188

[41] T. F. Cerqueira, S. Botti, A. San-Miguel, M. A. Marques, Density-functional tight-binding study of the collapse of carbon nanotubes under hydrostatic pressure, Carbon 69 (0) (2014) 355–360.

[42] J. P. Lu, Elastic properties of carbon nanotubes and nanoropes, Phys. Rev. Lett. 79 (1997) 1297–1300. doi:10.1103/PhysRevLett.79.1297.

[43] A. Krishnan, E. Dujardin, T. W. Ebbesen, P. N. Yianilos, M. M. J. Treacy, Young's modulus of single-walled nanotubes, Phys. Rev. B 58 (1998) 14013–14019. doi:10.1103/PhysRevB.58.14013.
URL https://link.aps.org/doi/10.1103/PhysRevB.58.14013

[44] A. Sood, P. Teresdesai, D. Muthu, R. Sen, A. Govindaraj, C. Rao, Pressure behaviour of single wall carbon nanotube bundles and fullerenes: A Raman study, Phys. Status Solidi B 215 (1) (1999) 393–401, International Conference on Solid State Spectroscopy - (ICSSS), Schwabisch Gmund, Germany, Sep 05-07, 1999. doi:{10.1002/(SICI)1521-3951(199909)215:1<393::AID-PSSB393>3.0.CO;2-8}.

[45] G. J. Piermarini, S. Block, J. Barnett, Hydrostatic limits in liquids and solids to 100 kbar, Journal of Applied Physics 44 (12) (1973) 5377–5382. arXiv:https://doi.org/10.1063/1.1662159, doi:10.1063/1.1662159.
URL https://doi.org/10.1063/1.1662159

[46] V. Hernndez, J. Casado, F. J. Ramrez, G. Zotti, S. Hotta, J. T. Lpez Navarrete, Efficient ? electrons delocalization in ?,???dimethyl

end?capped oligothiophenes: A vibrational spectroscopic study, The Journal of Chemical Physics 104 (23) (1996) 9271–9282. arXiv:https://doi.org/10.1063/1.471674, doi:10.1063/1.471674.
URL https://doi.org/10.1063/1.471674

[47] A. D. Esposti, O. Moze, C. Taliani, J. T. Tomkinson, R. Zamboni, F. Zerbetto, The intramolecular vibrations of prototypical polythiophenes, The Journal of Chemical Physics 104 (24) (1996) 9704–9718. arXiv:http://dx.doi.org/10.1063/1.471757, doi:10.1063/1.471757.
URL http://dx.doi.org/10.1063/1.471757

[48] A. Degli Esposti, F. Zerbetto, A density functional study of the vibrations of three oligomers of thiophene, The Journal of Physical Chemistry A 101 (39) (1997) 7283–7291. arXiv:https://doi.org/10.1021/jp971233o, doi:10.1021/jp971233o.
URL https://doi.org/10.1021/jp971233o

[49] J. Casado, V. Hernndez, S. Hotta, J. T. L. Navarrete, Vibrational spectra of charged defects in a series of α,α'-dimethyl end-capped oligothiophenes induced by chemical doping with iodine, The Journal of Chemical Physics 109 (23) (1998) 10419–10429. arXiv:http://dx.doi.org/10.1063/1.477697, doi:10.1063/1.477697.
URL http://dx.doi.org/10.1063/1.477697

[50] A. Jorio, A. G. S. Filho, Raman studies of carbon nanostructures, Annual Review of Materials Research 46 (1) (2016) 357–382. arXiv:http://dx.doi.org/10.1146/annurev-matsci-070115-032140, doi:10.1146/annurev-matsci-070115-032140.
URL http://dx.doi.org/10.1146/annurev-matsci-070115-032140

[51] M. Dresselhaus, G. Dresselhaus, A. Jorio, A. S. Filho, R. Saito, Raman spectroscopy on isolated single wall carbon nanotubes, Carbon 40 (12) (2002) 2043 – 2061. doi:http://dx.doi.org/10.1016/S0008-6223(02)00066-0.
URL //www.sciencedirect.com/science/article/pii/S0008622302000660

[52] M. Dresselhaus, G. Dresselhaus, R. Saito, A. Jorio, Raman spectroscopy of carbon nanotubes, Phys. Rep. 409 (2) (2005) 47–99.

695 doi:10.1016/j.physrep.2004.10.006.
URL http://www.sciencedirect.com/science/article/pii/S0370157304004570

[53] A. Jorio, A. G. Souza Filho, G. Dresselhaus, M. S. Dresselhaus, A. K. Swan, M. S. Ünlü, B. B. Goldberg, M. A. Pimenta, J. H. Hafner, C. M. 700 Lieber, R. Saito, G-band resonant raman study of 62 isolated single-wall carbon nanotubes, Phys. Rev. B 65 (2002) 155412. doi:10.1103/PhysRevB.65.155412.

[54] A. Jorio, M. A. Pimenta, A. G. S. Filho, R. Saito, G. Dresselhaus, M. S. Dresselhaus, Characterizing carbon nanotube samples with resonance 705 raman scattering, New J. Phys. 5 (1) (2003) 139.
URL http://stacks.iop.org/1367-2630/5/i=1/a=139

[55] A. L. Aguiar, E. B. Barros, R. B. Capaz, A. G. Souza Filho, P. T. C. Freire, J. Mendes Filho, D. Machon, C. Caillier, Y. A. Kim, H. Muramatsu, M. Endo, A. San-Miguel, Pressure-induced collapse in double-710 walled carbon nanotubes: Chemical and mechanical screening effects, J. Phys. Chem. C 115 (13) (2011) 5378–5384. doi:10.1021/jp110675e.

[56] A. C. Torres-Dias, T. F. Cerqueira, W. Cui, M. A. Marques, S. Botti, D. Machon, M. A. Hartmann, Y. Sun, D. J. Dunstan, A. San-Miguel, From mesoscale to nanoscale mechanics 715 in single-wall carbon nanotubes, Carbon 123 (2017) 145 – 150. doi:https://doi.org/10.1016/j.carbon.2017.07.036.
URL http://www.sciencedirect.com/science/article/pii/S0008622317307194

[57] A. L. Aguiar, A. San-Miguel, E. B. Barros, M. Kalbáč, D. Machon, 720 Y. A. Kim, H. Muramatsu, M. Endo, A. G. Souza Filho, Effects of intercalation and inhomogeneous filling on the collapse pressure of double-wall carbon nanotubes, Phys. Rev. B 86 (2012) 195410. doi:10.1103/PhysRevB.86.195410.

[58] W. Cui, T. F. T. Cerqueira, S. Botti, M. A. L. Marques, A. San-Miguel, 725 Nanostructured water and carbon dioxide inside collapsing carbon nanotubes at high pressure, Phys. Chem. Chem. Phys. 18 (2016) 19926–19932. doi:10.1039/C6CP03263J.
URL http://dx.doi.org/10.1039/C6CP03263J

[59] C. S. Wang, W. E. Pickett, Density-functional theory of excitation spectra of semiconductors: Application to si, Phys. Rev. Lett. 51 (1983) 597–600. doi:10.1103/PhysRevLett.51.597.
URL https://link.aps.org/doi/10.1103/PhysRevLett.51.597

[60] n. Morales-Garc a, R. Valero, F. Illas, An empirical, yet practical way to predict the band gap in solids by using density functional band structure calculations, The Journal of Physical Chemistry C 121 (34) (2017) 18862–18866. arXiv:https://doi.org/10.1021/acs.jpcc.7b07421, doi:10.1021/acs.jpcc.7b07421.
URL https://doi.org/10.1021/acs.jpcc.7b07421

[61] Y. Almadori, L. Alvarez, R. Le Parc, R. Aznar, F. Fossard, A. Loiseau, B. Jousselme, S. Campidelli, P. Hermet, A. Belhboub, A. Rahmani, T. Saito, J.-L. Bantignies, Chromophore ordering by confinement into carbon nanotubes, The Journal of Physical Chemistry C 118 (33) (2014) 19462–19468. arXiv:https://doi.org/10.1021/jp505804d, doi:10.1021/jp505804d.
URL https://doi.org/10.1021/jp505804d

[62] A. J. Ghandour, I. F. Crowe, J. E. Proctor, Y. W. Sun, M. P. Halsall, I. Hernandez, A. Sapelkin, D. J. Dunstan, Pressure coefficients of raman modes of carbon nanotubes resolved by chirality: Environmental effect on graphene sheet, Phys. Rev. B 87 (2013) 085416.

[63] B. Anis, K. Yanagi, C. Kuntscher, Optical microspectroscopy study on enriched (11,10) swcnts encapsulating c_{60} fullerene molecules, Carbon 107 (2016) 593 – 599. doi:http://dx.doi.org/10.1016/j.carbon.2016.06.026.
URL http://www.sciencedirect.com/science/article/pii/S0008622316304778

[64] A. Merlen, N. Bendiab, P. Toulemonde, A. Aouizerat, A. San Miguel, J. L. Sauvajol, G. Montagnac, H. Cardon, P. Petit, Resonant raman spectroscopy of single-wall carbon nanotubes under pressure, Phys. Rev. B 72 (2005) 035409. doi:10.1103/PhysRevB.72.035409.

[65] U. D. Venkateswaran, A. M. Rao, E. Richter, M. Menon, A. Rinzler, R. E. Smalley, P. C. Eklund, Probing the single-wall carbon nanotube

bundle: Raman scattering under high pressure, Phys. Rev. B 59 (1999) 10928–10934. doi:10.1103/PhysRevB.59.10928.

[66] M. Yao, Z. Wang, B. Liu, Y. Zou, S. Yu, W. Lin, Y. Hou, S. Pan, M. Jin, B. Zou, T. Cui, G. Zou, B. Sundqvist, Raman signature to identify the structural transition of single-wall carbon nanotubes under high pressure, Phys. Rev. B 78 (20) (2008) 205411. doi:10.1103/PhysRevB.78.205411.

[67] A. L. Aguiar, R. B. Capaz, A. G. Souza Filho, A. San-Miguel, Structural and phonon properties of bundled single- and double-wall carbon nanotubes under pressure, J. Phys. Chem. C 116 (42) (2012) 22637–22645. doi:10.1021/jp3093176.

[68] C. Caillier, D. Machon, A. San-Miguel, R. Arenal, G. Montagnac, H. Cardon, M. Kalbac, M. Zukalova, L. Kavan, Probing high-pressure properties of single-wall carbon nanotubes through fullerene encapsulation, Phys. Rev. B 77 (12) (2008) 125418. doi:10.1103/PhysRevB.77.125418.

[69] Y. Almadori, L. Alvarez, R. Le Parc, R. Aznar, F. Fossard, A. Loiseau, B. Jousselme, S. Campidelli, P. Hermet, A. Belhboub, A. Rahmani, T. Saito, J.-L. Bantignies, Chromophore ordering by confinement into carbon nanotubes, The Journal of Physical Chemistry C 118 (33) (2014) 19462–19468. arXiv:http://dx.doi.org/10.1021/jp505804d, doi:10.1021/jp505804d.
URL http://dx.doi.org/10.1021/jp505804d

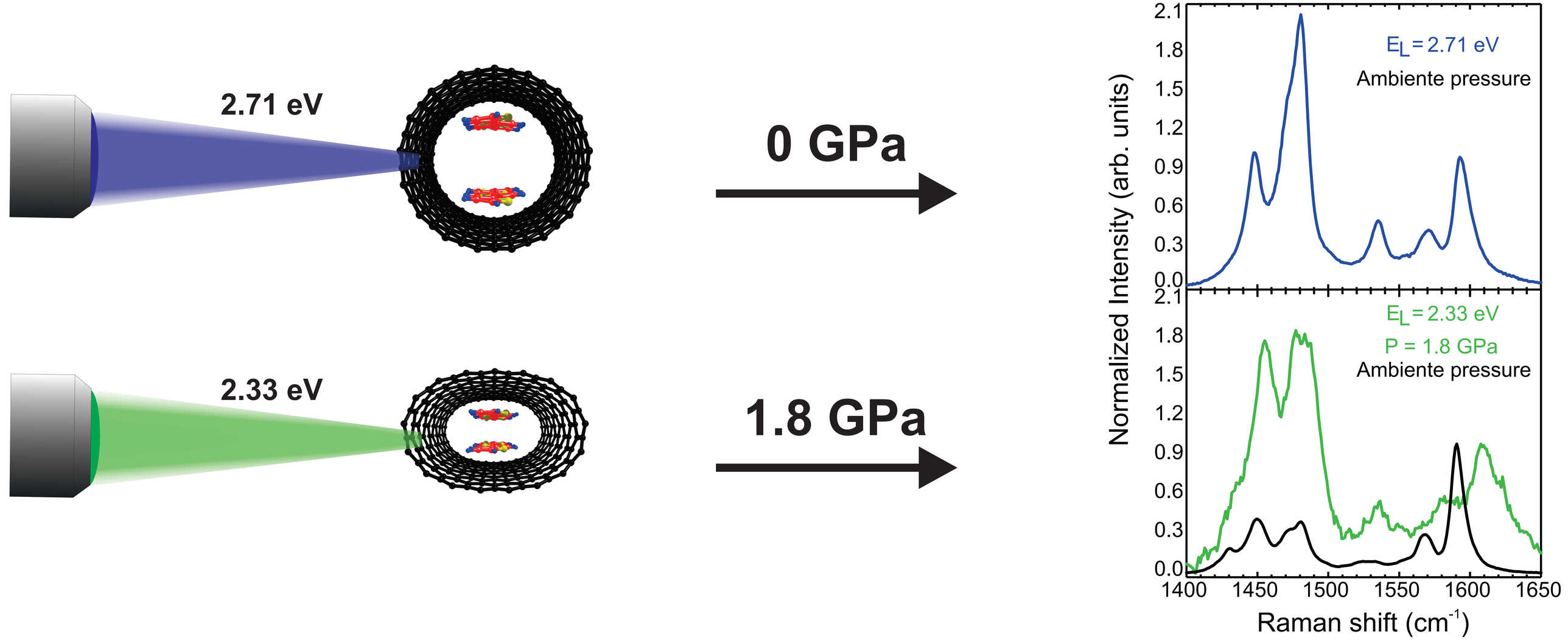
2.71 eV
0 GPa
2.33 eV
1.8 GPa
E_L = 2.71 eV
Ambiente pressure
E_L = 2.33 eV
P = 1.8 GPa
Ambiente pressure
Normalized Intensity (arb. units)
Raman shift (cm^{-1})
0.0
0.3
0.6
0.9
1.2
1.5
1.8
2.1
1400
1450
1500
1550
1600
1650